Bulletin of the Seismological Society of America, Vol. 84, No. 1, pp. 142–148, February 1994

Sources of Primary and Secondary Microseisms

by Robert K. Cessaro

Abstract Low-frequency (0.01 to 0.2 Hz) seismic noise, arising from pelagic storms, is commonly observed as microseisms in seismic records from land and ocean bottom detectors. One principal research objective, in the study of microseisms, has been to locate their sources. This article reports on an analysis of primary and secondary microseisms (i.e., near and double the frequency of ocean swell) recorded simultaneously on three land-based long-period arrays (Alaskan Long Period Array, Montana Large Aperture Seismic Array, and Norwegian Seismic Array) during the early 1970s. Reliable microseism source locations are determined by wide-angle triangulation, using the azimuths of approach obtained from frequency-wave number analysis of the records of microseisms propagating across these arrays. Two near-shore sources of both primary and secondary microseisms appear to be persistent in the sense that they are associated with essentially constant near-shore locations. Secondary microseisms are observed to emanate from wide-ranging pelagic locations in addition to the same near-shore locations determined for the primary microseisms.

Introduction

Microseisms, the persistent oscillations of seismic waves unrelated to earthquakes, explosions or local noise sources, have been observed on seismic records since the 19th century (Bertelli, 1872). Since then, locating their source has been a fundamental research goal in their study. Studies early in this century proposed their association with meteorological storm systems in the ocean. More recently, numerous observations have been made both on land and on the ocean bottom. Microseisms are characterized by long-period waves with dominant periods between 2 and 40 sec. These waves have been interpreted as short-period P waves, higher mode surface waves, long-period surface waves, and ultra-long-period surface waves. Microseisms propagating as long-period surface waves were identified by Haubrich *et al.* (1963) as primary- and double-frequency (or secondary) microseisms, covering two distinctly different frequency bands: 80 and 150 mHz, respectively. The association of primary and secondary microseisms with the same atmospheric disturbance was first noted by Oliver and Page (1963) who also observed that primary microseisms have twice the dominant periods of the related secondary microseisms. Several mechanisms for the generation of these two types of microseisms have been postulated in recent work.

Primary microseisms are observed between ~40 and 80 mHz on land (e.g., Oliver, 1962; Oliver and Page, 1963; Haubrich *et al.*, 1963; Haubrich and McCamy, 1969; Darbyshire and Okeke, 1969) and on the ocean bottom (e.g., Barstow *et al.*, 1989; Sutton and Barstow, 1990). Their spectral peak reflects the frequencies of the dominant ocean waves and appear to form in shallow water by the interaction of ocean swells with a shoaling ocean bottom (Oliver, 1962; Haubrich *et al.*, 1963).

Secondary- or double-frequency microseisms are commonly observed, with dominant peak frequencies between 100 and 160 mHz or approximately double that of the peak ocean wave frequencies. They are observed on land (e.g., Bernard 1941; Iyer, 1958; Darbyshire, 1950; Hasselmann, 1963, Haubrich *et al.*, 1963) and may be generated in either shallow or deep water. An early theoretical work by Miche (1944) suggested that low-frequency sea-bottom pressure perturbations could be generated by the nonlinear interaction of surface ocean waves. Expanding on Miche's work, Longuet-Higgins (1950) proposed that double-frequency microseisms arise from nonlinear second-order pressure perturbations on the ocean bottom caused by the interference of two ocean waves of equal wavelengths traveling in opposite directions. In a study of double-frequency microseisms recorded at the Large Aperture Seismic Array (LASA), Haubrich and McCamy (1969) concluded that they result primarily from coastal reflection of ocean waves.

Several studies have shown that the ocean-bottom microseism spectrum is similar in shape to the continental microseismic spectrum, but with greater amplitude, and correlates well with known storm systems (Bradner and Dodds, 1964; Bradner *et al.* 1965, 1970;

Latham and Sutton, 1966; Latham and Nowroozi, 1968; Sutton and Barstow, 1990). Analysis of Ocean Bottom Seismometer (OBS) data recorded near a cyclonic source suggests that microseisms arise from nonlinear interaction of storm waves (Ostrovsky and Rykunov, 1982).

Most recent studies of microseisms have attempted to determine the directions of approach, phase velocity, and location of the source, and in some cases, to study structural and sediment properties (Darbyshire, 1954; Iyer, 1958; Toksöz, 1964; Latham and Nowroozi, 1968; Bossolasco *et al.*, 1973; Asten and Henstridge, 1984; Yamamoto and Torii, 1986; Barstow *et al.*, 1989; Sutton and Barstow, 1990). Microseisms appear to propagate mainly by Rayleigh wave motion but may contain Love wave components where propagation is through uninterrupted layered structure (Rind and Donn, 1979).

Analysis of low-frequency land-recorded seismic array data has provided a better understanding of the nature of the low-frequency noise (seismic and acoustic) generated by large pelagic storms that propagates into the continental interior as microseismic surface waves. Haubrich and McCamy (1969) and Toksöz and Lacoss (1968) studied frequency wavenumber spectra of microseism recordings at the LASA to detail microseismic sources and propagation modes. Capon (1972), suggested the coincidence of an atmospheric low-pressure region with a microseism source determined from simultaneous frequency-wavenumber (f-k) analysis of the LASA and the Alaskan Long Period Array (ALPA) long-period data. Other studies using small array data have been used to examine microseismic surface wave sources (e.g., Szelwis 1980, 1982). From analysis of a 3-day sample of primary microseisms obtained from two large-aperture arrays, Cessaro and Chan (1989) found two near-shore source locations that were associated with nearly all of the coherent primary microseisms propagating across two arrays.

This article reports on the progress of research begun in 1988 (Cessaro and Chan, 1989). The current study extends the analysis to secondary microseisms with a larger sample of microseisms, and it includes the redundancy afforded by one additional array. The expanded observations of primary microseisms have provided confirmation of the preliminary results showing two persistent near-shore sources of primary microseism noise that are clearly associated with pelagic storm systems but not as a close function of their locations (Cessaro and Chan, 1989). In addition, secondary microseism sources are also observed from the same two persistent northern hemisphere near-shore locations but are also observed to emanate from other ephemeral pelagic sources more closely related to storm locations.

Data Description

The low-frequency microseism signals are obtained from digitized recordings collected by the LASA, the ALPA, and the Norwegian Seismic Array (NORSAR) for the period 00:00 UTC 25 November 1973 to 00:00 UTC 29 November 1973. The LASA, operating from 1965 through 1978, included 21 three-component long-period seismometers. The ALPA, operating from 1970 through 1982, was composed of 19 long-period triaxial seismometers. The NORSAR included 22 long-period seismometers during the operating period 1971 to 1976. The arrays recorded digitally at 1-Hz sampling frequency. The frequency response of the long-period elements of the arrays is flat to velocity from 25- to 200-sec period (5 to 40 mHz). The location and pattern of each array are shown in Figure 1. The differences in array dimensions and geometries are reflected in the resolution observed in the f-k analysis of their respective data.

Continuous 4000-sec data samples are excerpted for analysis on an interval of approximately 6 hrs from the long-period array data archive (Teledyne Geotech Alexandria Laboratories). Signals are taken from vertical-component channels for LASA and NORSAR and mathematically rotated vertical component channels for ALPA. Signals are bandpass filtered using a four-pole Butterworth filter centered at 16 sec (0.06 Hz) and 8 sec (0.12 Hz) for the single- and double-frequency microseism bands, respectively, so that visual comparisons of the microseism signals with the f-k analysis results may be more easily be made. Instrument corrections (nominally 25-sec peak response) proved unnecessary for the f-k analysis.

Some of the data samples are shifted by as much as an hour from the regular 6-hr interval to avoid large earthquake phases exhibiting substantial power in the same

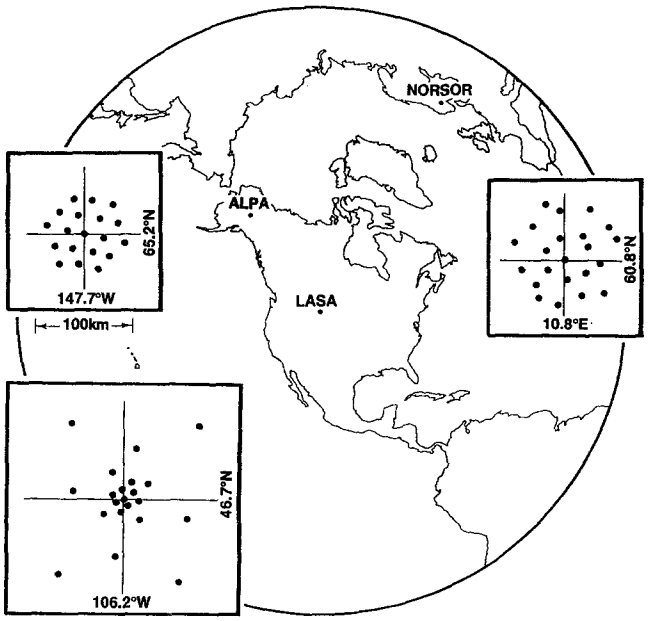

Figure 1. The location and patterns of LASA, NORSAR, and ALPA seismic arrays (drawn to the same scale).

pass bands. These earthquake phases are confirmed on the International Seismological Centre (ISC) *Bulletin* reporting origin times and hypocenters. Although these phases are not directly useful to the objective of this study, they do provide an indirect means of calibrating the accuracy of the microseism approach azimuths obtained from the f-k analysis. Earthquake phases, examined in the microseism frequency bands, give approach azimuths that are typically within one degree of the theoretical azimuth over the range of azimuths encountered for the microseisms.

Analysis

Frequency-Wavenumber Analysis

f-k analysis is performed on samples of low-frequency ambient noise recorded during the activity of a series three pelagic storm systems to determine dominant phase velocities and approach azimuths. The ambient noise field recorded during the study period consists of both coherent and incoherent components. The incoherent component does not appear as separable power peaks in the f-k analysis. The coherent component consists of microseisms from multiple sources and earthquakes. The sampled time periods are selected by searching the Mariners Weather Log (1973) covering the northern hemisphere peak storm months for the presence of isolated principal cyclone tracks occurring simultaneously in the North Atlantic and the North Pacific oceans while the three seismic arrays were in full operation.

Microseisms arriving as surface waves from pelagic storms are examined for temporal and spatial variation in phase velocity and direction of approach by using a sliding-window, broadband f-k analysis technique (Capon, 1969) on 4000-sec bandpassed digitized array data samples. The term "f-k analysis" is used here as a convenience; it is more accurately referred to as frequency-slowness analysis, because the frequency-wavenumber power spectra are examined for specific bandlimited frequency planes. f-k analysis is performed on sequential 128-sec data segments in the 4000-sec data sample. Signal time windows are advanced by 100 sec from previous windows, resulting in adjacent window overlaps of 28 sec. Resulting estimates of approach azimuth and phase velocity are collected and examined for consistency and distribution. Figure 2 shows an example of the results of f-k processing. The contours shown represent 1-dB increments in power referred to the window maximum for a given frequency band. Multiple f-k power peaks obtained from each 4000-sec data sample provide many approach azimuths that contribute to the suite of potential microseismic source locations. Because the microseisms are observed to propagate in the form of Rayleigh waves, the approach azimuths used are limited to those attended by phase velocity observations between 3.0 and 4.0 km/sec (e.g., Capon, 1970; Cessaro and Chan, 1989). Time windows containing low-frequency phases from known earthquakes are excluded from this analysis.

Spectral Analysis

Averaged spectra obtained for signals from one vertical component in each array show that power in the two microseism bands correlates well with storm intensity (e.g., Korhonen and Pirhonen, 1976). The variations in spectral power and peak frequencies are consistent with the storm intensities reported in the Mariners Weather Log (1973). An order of magnitude fluctuation in both the primary and secondary microseism amplitudes is typically observed over a time scale of minutes during the passage of these storms.

The spectra observed in each array record represent a composite of distant and local sources. Incoherent local spectral components are reduced as the spectra are averaged. Spectral components from the activity of distant storms occurring simultaneously in the Atlantic and Pacific oceans can be visually enhanced by averaging,

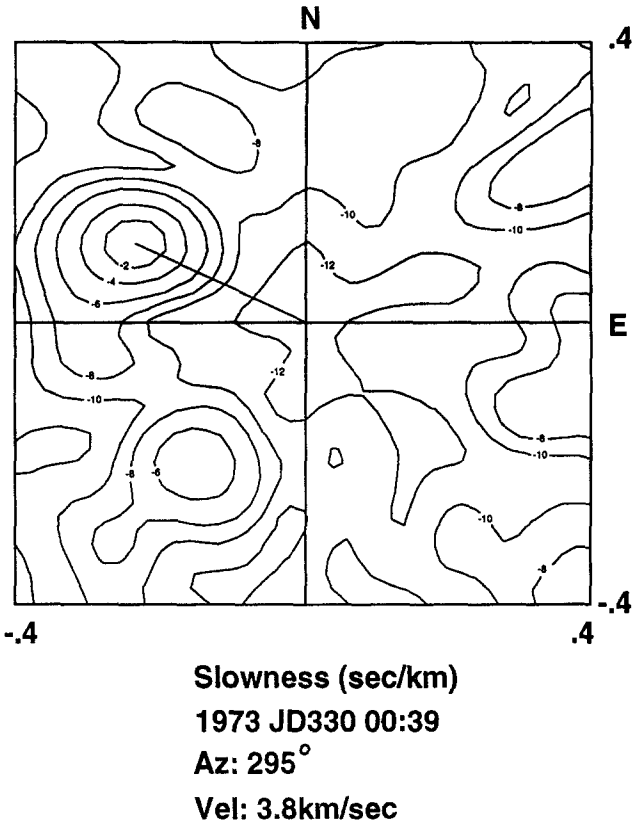

Figure 2. Example of the results of frequency-wavenumber processing for single-frequency microseism signals recorded on the NORSAR array. The contours shown represent 2-dB increments in power referred to the window maximum for the 0.04 to 0.08-Hz frequency band. The coordinates are in units of slowness in x and y.

particularly if they can be further separated by beam forming on their respective approach azimuths. The time history of primary microseism spectra, observed over a time period where two storms are active, can be separated by noting the primary microseism spectra and associated dominant frequency-wavenumber power peaks for the same data window. The separation of spectral components from independent storm-generated sources is improved by beam forming on the azimuth associated with one of the dominant frequency-wavenumber peaks at a time when the other peak appears temporarily weak or absent (Fig. 3). In general, microseisms arising from the action of several storms exhibit different spectral characteristics and temporal variations that can be followed separately in the time history of their respective power spectra. It can be adduced from this analysis that the approach azimuths determined for these data samples are from storm-generated microseisms evident in the time series record rather than from any localized source.

Obtaining Microseism Source Locations by Triangulation

A wide-aperture triangulation is performed on simultaneous approach azimuth observations made from ALPA, LASA, and NORSAR data by combining the estimates of approach azimuths obtained from the f-k analysis over each 4000-sec data sample. This approach represents an improvement in resolution of distance and azimuth between sources and receivers compared with that obtained from earlier array studies (Toksöz and Lacoss, 1968; Lacoss *et al.*, 1969; Capon, 1969, 1970, 1972). Most earlier array studies did not attempt to triangulate and so provided only limited information on distance from source to receiver. The estimates of azimuth and velocity stability and associated errors are obtained from the distribution of approach azimuths, velocity, and their corresponding frequency-wavenumber power. In this way, each 4000-sec data sample provides several representative approach azimuths along with corresponding estimates of their reliability. Figure 4 shows the distribution of primary microseism approach azimuths determined for all of the time windows used during the experimental period. The intersection of separate map projections of these azimuths and error estimates from their respective arrays provide bounding estimates of the

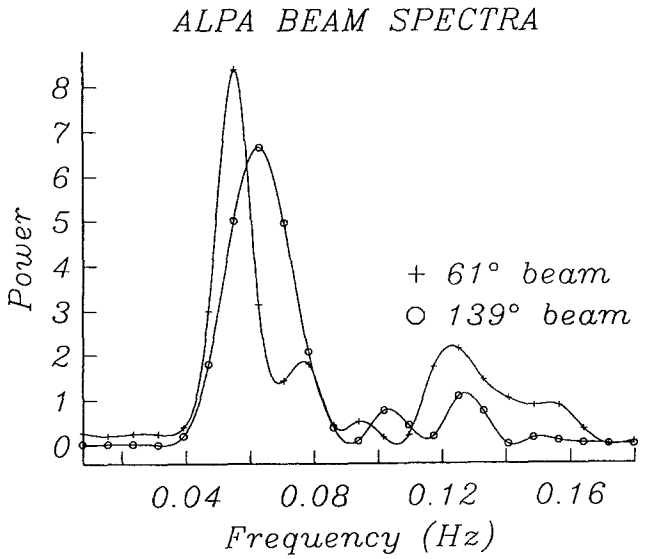

Figure 3. Example of the microseism spectra enhanced by beam forming on azimuths associated with each of the dominant primary microseism frequency-wavenumber peaks at a time when the other peak is temporarily weak or absent. The power is shown in decibels relative to an arbitrary reference, and the spectra are corrected for instrument response.

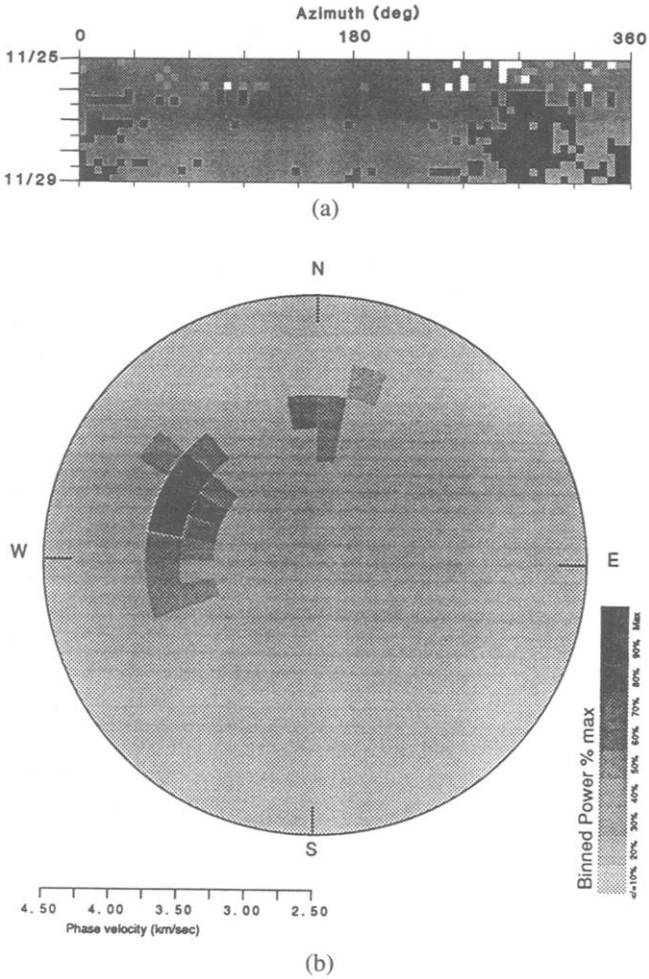

Figure 4. Example of the binned distribution of primary microseism approach azimuths determined with data for time windows used during the period 25 November 1973 to 29 November 1973 for NORSAR array. (a) Power-weighted frequency-wavenumber peaks by azimuth and time (5° azimuth bin); (b) power-weighted frequency-wavenumber peaks by azimuth and velocity (5° azimuth, 0.25 km/sec velocity bins).

microseism source location. Estimates from three arrays is most useful, because it provides some redundancy in the technique.

Results and Discussion

Both primary and secondary microseism spectral power are observed to vary by more than an order of magnitude over a time scale of minutes. Modulation of their corresponding frequency-wavenumber power peaks is qualitatively consistent with the spectral power variations. The existence of multiple storms during the sampled data times is reflected in the peak frequencies observed, i.e., microseisms from each storm exhibited distinctive peak frequency histories as their surface winds developed, moved, and dissipated. The sliding-window technique applied to f-k analysis provides temporal and spatial information about the microseism sources, factors particularly important for characterizing secondary microseisms.

f-k analysis may be regarded as a measure of microseismic wave field coherency, in the sense that it detects the coherent fraction of the total noise field. Primary microseisms are associated with deterministic sources that appear to be spatially limited to a few near-shore locations. Secondary microseism sources appear to be both deterministic and stochastic in the sense that they are associated with both spatially limited coastal locations and oceanic sources that are only weakly related to the storm trajectory.

Primary Microseism Sources

Wide-angle triangulation using approach azimuths obtained by these methods confirms the results of preliminary work (Cessaro and Chan, 1989) and shows that primary microseisms emanate from persistent near-shore locations that do not correlate well with their associated pelagic storm locations. During the time period sampled for this study, three major storms were active in the North Pacific and Atlantic oceans and two primary microseism source locations are identified: (1) A wide ranging North Pacific storm correlates with a microseism source near the west coast of the Queen Charlotte Islands, British Columbia, and (2) Two North Atlantic storms correlate well with a source near the coast of Newfoundland (Fig. 5). Although the North Pacific storm trajectory subtends an arc greater than 90° from the ALPA, the associated primary microseism source appears to be stable within about 5° (Fig. 5). The microseism source near Newfoundland exhibits similar stability.

Secondary Microseism Sources

Secondary microseisms radiate from the same near-coastal sources observed for primary microseisms, and in addition, are observed arriving from meandering (time-variant) oceanic sources. The oceanic sources are broadly

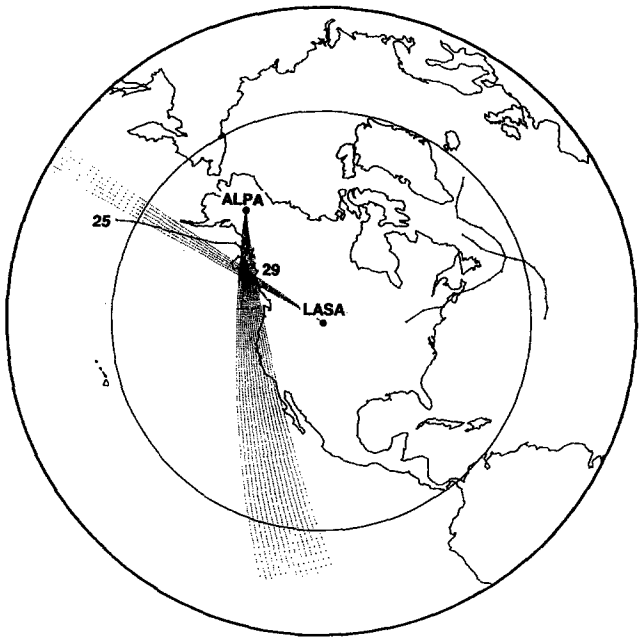

(a)

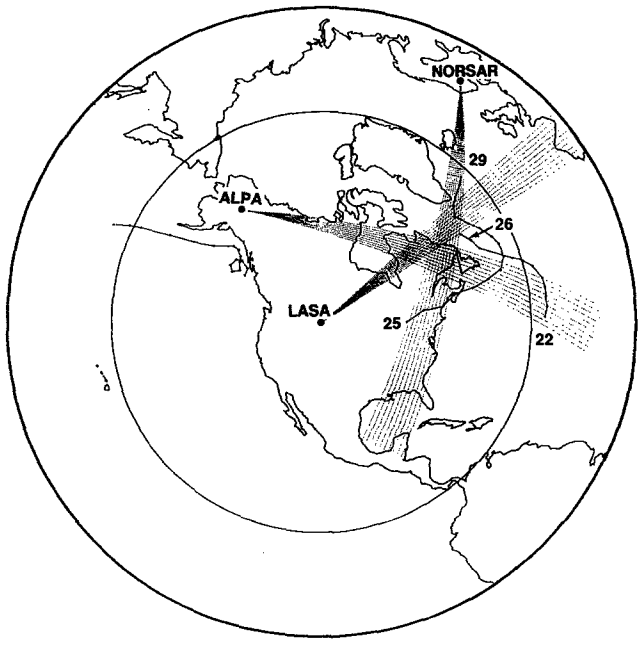

(b)

Figure 5. Maps showing the two persistent primary microseism source locations determined by wide-angle triangulation of approach azimuths. Projection widths are drawn from the half-power bounds in the approach azimuth distribution. (a) North Pacific storms are associated with a microseism source near the west coast of the Queen Charlotte Islands; (b) North Atlantic storms generate result in sources located near the coast of Newfoundland.

associated with the storm trajectory, in the sense that the locations obtained through triangulation remain within the synoptic area of the storm path. For example, a storm path in the western North Atlantic is attended by secondary microseism sources that also appear to be in that region. Locating the oceanic sources of secondary microseisms by triangulation is complicated by their spatial variability over a time scale on the same order as the data sample windows. Once a trial triangulation position is determined for a given data sample window, the implied differences in travel times to the arrays are considered and the appropriate data windows are adjusted to ensure that the trial location is remains consistent. This problem does not arise for the time-invariant near-coastal microseism source. The positions shown in Figure 6 are obtained by triangulation considering travel time differences.

Conclusion

Although pelagic storms provide the source of microseismic wave energy, it is the interplay among (1) the pelagic storm parameters, such as tracking velocity, peak wind speed, location, effective area, and ocean surface pressure variation, (2) the resulting storm waves and their frequency distribution, (3) the direction of storm wave propagation, and (4) the near-shore and deep-ocean processes that control the production of microseisms. It is probable that only a fraction of the total storm-related noise field is coherent. From the perspective of a seismic array, at any given moment only the most energetic coherent portion of the noise field is detected by f-k analysis, i.e., a peak in the frequency-wavenumber power represents the most energetic coherent portion of the microseismic wave field at that instant. f-k analysis is sensitive, therefore, to only a small part of the total noise field. It is also shown that both the primary and secondary microseism source locations do not appear to follow the storm trajectories directly. Secondary microseism source locations exhibit a duality in the sense that the near-shore source is shared by the primary microseism source while the other meanders within the synoptic region of peak storm wave activity. From the several storms analyzed so far, it appears that the observed relationships between the changing storm parameters and resulting shifts in secondary microseisms locations are typical. It is not known why particular near-shore locations radiate strong coherent primary and secondary microseisms. It may be a combination of local resonance modes and storm wave approach and reflection interactions. There appear to be at least two specific near-shore regions in the northern hemisphere that generate microseisms strong enough to be observed as persistent frequency-wavenumber power peaks in both the secondary and primary microseism bands regardless of the storm location within the associated North Atlantic or Pacific ocean basin, provided the storm-generated surface water waves are sufficiently energetic. Preliminary analysis of microseisms recorded during the peak storm periods for the southern hemisphere suggests the existence of persistent sources there also (Cessaro, 1991).

Figure 6. Map showing the positions of secondary microseism sources for storms in the north Pacific and Atlantic oceans, obtained by triangulation considering travel time differences. Position boundaries are drawn from the projection of half-power limits in the approach azimuth distribution determined for data from each array. The numbers refer to the sample sequence number for an interval spacing of 6 hr over the period 25 November 1973 to 29 November 1973.

Acknowledgments

The clarity of this article was improved by careful review by G. Sutton and F. Duennebier. The research was funded by the Office of Naval Research under several contracts while the author was affiliated with Teledyne Geotech.

References

Asten, M. W. and J. D. Henstridge (1984). Array estimators and the use of microseisms for reconnaissance of sedimentary basins, *Geophysics* **49**, 1828–1837.

Barstow, N., G. H. Sutton, and J. A. Carter (1989). Particle motion and pressure relationships of ocean bottom noise at 3900 m depth: 0.003 to 5 Hz, *Geophys. Res. Let.* **16**, 1185–1188.

Bernard, P. (1941). Sur certaines proprietes de la houle etudiees a l'aide des enregistrements seismographiques, *Bull. Inst. Oceanogr. Monaco* **800**, 1–19.

Bertelli, T. (1872). Osservazoni sui piccoli movimenti dei pendoli in relazione ad alucuni fenomeni meteorologiche, *Boll. Meteorol. Osserv. Coll. Roma* **9**, 10 pp.

Bossolasco, M., G. Cicconi, and C. Eva (1973). On microseisms recorded near a coast, *Pure Appl. Geophys.* **103**, 332–346.

Bradner, H., L. de Jerphanion, and R. Langlois (1970). Ocean microseism measurements with a neutral buoyancy free-floating midwater seismometer, *Bull. Seism. Soc. Am.* **60**, 1139–1150.

Bradner, H. and J. G. Dodds (1964). Comparative seismic noise on the ocean bottom and on land, *J. Geophys. Res.* **69**, 4339–4348.

Bradner, H., J. G. Dodds, and R. E. Foulks (1965). Investigation of microseism sources with ocean-bottom seismometers, *Geophysics* **30**, 511–526.

Capon, J. (1969). High resolution frequency-wavenumber spectrum analysis, *Proc. IEEE* **57**, 1408–1418.

Capon, J. (1970). Analysis of Rayleigh-wave multipath propagation at LASA, *Bull. Seism. Soc. Am.* **60**, 1701–1731.

Capon, J. (1972). Long-period signal processing results for LASA, NORSAR and ALPA, *J. R. Astr. Soc.*, **31**, 279–296.

Cessaro, R. K. (1991). Seismic array study of primary and secondary microseisms, *EOS* **72**, 302–303.

Cessaro, R. K. and W. W. Chan (1989). Wide-angle triangulation array study of simultaneous primary microseism sources, *J. Geophys. Res.* **94**, 15,555–15,563.

Darbyshire, J. (1950). Identification of microseismic activity with sea waves, *Proc. R. Soc. Lond. Ser. A* **202**, 439–448.

Darbyshire, J. (1954). Structure of microseismic waves: Estimation of direction of approach by comparison of vertical and horizontal components, *Proc. R. Soc. Lond. Ser. A* **223**, 96–111.

Darbyshire, J. and E. O. Okeke (1969). A study of primary and secondary microseisms recorded in Anglesey, *Geophys. J. R. Astr. Soc.* **17**, 63–92.

Hasselmann, K. (1963). A statistical analysis of the generation of microseisms, *Rev. Geophys. Space Phys.* **1**, 177–210.

Haubrich, R. A. and K. McCamy (1969). Microseisms: coastal and pelagic sources, *Rev. Geophys. Space Phys.* **7**, 539–571.

Haubrich, R. A., W. H. Munk, and F. E. Snodgrass (1963). Comparative spectra of microseisms and swell, *Bull. Seism. Soc. Am.* **53**, 27–37.

Iyer, H. M. (1958). A study of direction of arrival of microseisms at Kew Observatory, *Geophys. J.* **1**, 32–43.

Korhonen, H. and S. E. Pirhonen (1976). Spectral properties and source areas of storm microseisms at NORSAR, Scientific Report 2-75/76 Teledyne Geotech, Alexandria, Virginia.

Lacoss, R. T., Kelley, E. J., Toksös, M. N. (1969). Estimation of seismic noise signals using arrays, *Geophysics*, **34**, 21–36.

Latham, G. V. and A. A. Nowroozi (1968). Waves, weather, and ocean bottom microseisms, *J. Geophys. Res.* **73**, 3945–3956.

Latham, G. V. and G. H. Sutton (1966). Seismic measurements on the ocean floor, 1. Bermuda Area, *J. Geophys. Res.* **71**, 2545–2573.

Longuet-Higgins, M. S. (1950). A theory of the origin of microseisms, *Philos. Trans. R. Soc. London* **243**, 1–35.

Miche, M. (1944). Mouvements ondulatoires de la mer en profondeur constante ou decroissante, *Annales des Ponts et Chaussees* **114**, 25–78.

Oliver, J. (1962). A worldwide storm of microseisms with periods of about 27 seconds, *Bull. Seism. Soc. Am.* **52**, 507–517.

Oliver, J. and R. Page (1963). Concurrent storms of long and ultralong period microseisms, *Bull. Seism. Soc. Am.* **53**, 15–26.

Ostrovsky, A. A. and L. N. Rykunov (1982). Experimental study of ocean bottom seismic noise during passage of a cyclone, *Oceanology* **22**, 720–722.

Rind, D. and W. Donn (1979). Microseisms at Palisades, 2, Rayleigh wave and Love wave characteristics and the geologic control of propagation, *J. Geophys. Res.* **84**, 5632–5642.

Sutton, G. H. and N. Barstow (1990). Ocean-bottom ultralow-frequency (ULF) seismo-acoustic ambient noise: 0.002 to 0.4 Hz, *J. Acoust. Soc. Am.* **87**, 2005–2012.

Szelwis, R. (1980). Inversion of microseismic array cross spectra, *Bull. Seism. Soc. Am.*, **70**, 127–148.

Szelwis, R. (1982). Modeling of microseismic surface wave sources, *J. Geophys. Res.* **87**, 6906–6918.

Toksöz, M. N. (1964). Microseisms and an attempted application to exploration, *Geophysics* **29**, 154–177.

Toksöz, M. N. and R. T. Lacoss (1968). Microseisms: mode structure and sources, *Science* **159**, 872–873.

U. S. Dept. of Commerce, NOAA, National Environmental Satellite, Data and Information Service (1973). Mariners Weather Log, U. S. Government Printing Office, Washington, D.C.

Wiechert, E. (1904). Verhandlungen der Zweiten Internationalen Seismologischen Konferenz, *Gerl. Beitr. Geophys. Erganzungsbd.* **2**, 41–43.

Yamamoto, T., and T. Torii (1986). Seabed shear modulus profile inversion using surface gravity (water) wave-induced bottom motion, *Geophys. J. R. Astr. Soc.* **85**, 413–431.

Pacific Tsunami Warning Center
91-270 Fort Weaver Rd.
Ewa Beach, Hawaii 96706

Manuscript received 19 February 1992.